# Silicon based optical pulse shaping and characterization

Ozdal Boyraz, Xinzhu Sang, En-Kuang Tien, Qi Song, Feng Qian and Metin Akdas
Department of Electrical Engineering & Computer Science, University of California, Irvine, CA, USA 92697

## ABSTRACT

The high-index contrast between the silicon core and silica cladding enable low cost chip-scale demonstration of all-optical nonlinear functional devices at relatively low pump powers due to strong optical confinement the in silicon waveguides. So far, broad ranges of applications from Raman lasers to wavelength converters have been presented. This presentation will highlight the recent developments on ultrafast pulse shaping and pulse characterization techniques utilizing the strong nonlinear effects in silicon. In particular, pulse compression due to two photon absorption and dual wavelength lasing and ultrafast pulse characterization based on XPM FROG measurement will be highlighted.
**Keywords:** Mode-locking, silicon waveguide, ultrafast nonlinear optics, Raman laser.

## 1. INTRODUCTION

Silicon photonics has become a rapidly growing field because of its possible dense on-chip integration with microelectronics and significant advances in nonlinear effects. Silicon waveguide is a good nonlinear medium because of two major reasons: First, due to the high-index contrast between the silicon core and silica cladding, silicon waveguides allow strong optical confinement. Second, silicon inherent a large effective nonlinearity compared to silica. It is possible to demonstrate low cost chip-scale of all-optical nonlinear functional devices at relatively low pump powers in silicon-on-insular (SOI) waveguide. In fact, nonlinear photonic phenomena and devices in silicon, such as Raman amplification and lasing [1-4], optical modulation [5-6], wavelength conversion [7-9], all-optical switching [10-12], pulse compression [13-14], control of slow light [15-16] and so on, have been successfully demonstrated. On the other hand, two-photon absorption (TPA) and TPA-induced free carrier absorption (FCA) are nonlinear losses dominating at high intensities and have been considered as detrimental effects and main obstacle in realizing high efficiency nonlinear photonic silicon devices. However, engineered use of TPA and FCA may increase the capabilities of silicon photonics in different applications [13, 17].

So far, the nonlinear optics in silicon focuses on three major areas. In the first area of silicon photonics strong Raman effect has been utilized to demonstrate lasing and amplification, and Raman based wavelength conversion at wavelengths starting from 1400nm up to 4000nm [18-20]. In the second area, Kerr nonlinearity with dispersion engineering has been heavily investigated to illustrate parametric wavelength conversion and nonlinear phase modulation [21-30]. Although, it is detrimental to aforementioned applications, TPA and FCA have been investigated to promote devices utilizing the free carrier plasma effect and transient properties of free carrier absorption [31-32].

Here a brief overview of recent development in silicon photonics is presented. In the first part, recent development in silicon Raman devices will be summarized. The second part of the paper focuses on the devices utilizing the Kerr nonlinearity. In the third part, we will present the recent developments in devices focusing on two photon process and free carrier absorption.

Optical Components and Materials VI, edited by Shibin Jiang, Michel J. F. Digonnet,
John W. Glesener, J. Christopher Dries, Proc. of SPIE Vol. 7212, 72120U
 · doi: 10.1117/12.810858

## 2. SILICON RAMAN DEVICES

Silicon is an indirect bandgap semiconductor and the light emission efficiency is very low. However, inherent strong Raman scattering is a way to overcome this restriction and make silicon to generate and amplify light. Since it was proposed in 2002, the silicon Raman devices attained fast track record. Since the demonstration of first silicon Raman laser in 2004 by the UCLA group [3], now chip scale Raman lasers can generate and amplify light at wavelengths from 1400nm to 4000nm. The main obstacle to silicon Raman devices is the attenuation induced by free carriers. One way to avoid free carrier is to operate the device in mid-IR wavelength (<2.2μm) such that TPA does not exist. A proof of concept experiment demonstrates mid-Infrared Raman amplifiers with high gain over a 1cm long silicon sample [18]. Here, 12dB on-off gain on signal at 3.39 μm has been achieved when the silicon sample is pumped by a 2.88 μm laser generated from optical parametric oscillator, Fig. 1(a). This technology extends the working wavelength in silicon photonic devices to near-IR and mid–IR regime. Alternatively, waveguides with p-i-n diode structures have been proposed and demonstrated to reduce the free carrier absorption [4]. Here, the free carrier accumulation is controlled by carrier sweep out by applying reverse on the pn diode over the waveguide. With increasing efficiency by loss reduction, Intel achieved a cascade wavelength Raman laser in silicon in an SOI rib waveguide with racetrack structure. In this configuration, the pump signal is coupled by the directional couplers to a straight waveguide, Fig. 2(a), which then generates 15.6 THz red shifted stimulated Raman scattering and creates first order Raman laser. Similarly, the first order Raman laser can generate second order Stokes shift and provide second order Raman laser at 1848nm, as shown in Fig. 2(b). Demonstration of Raman amplifier and Raman laser in Mid-IR wavelength pave the way to extend the communication wavelength and realization of cheap compact photonic devices up to Mid-IR wavelengths.

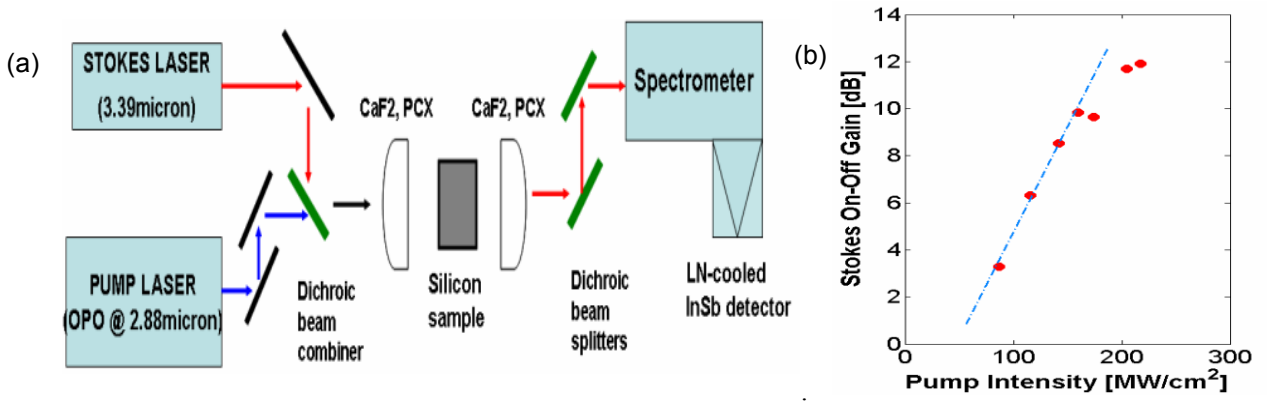


Fig. 1 (a) Experimental setup for mid-IR optical amplifier and (b)Raman gain as function of the pump intensity [19]

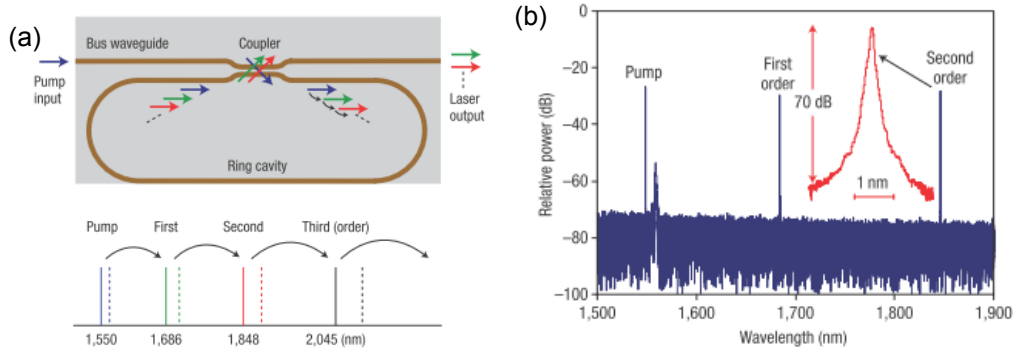


Fig. 2 (a) The racetrack ring laser cavity. The lower part illustrate the cascade lasing process and (b) the total output of the spectrum of the cascade laser. [20]

## 3. KERR NONLINEARITY IN SILICON

Similar to Raman effect the nonlinear index ($n_2$=5m$^2$/W at 1500nm) in silicon is 2 orders of magnitude larger than that of silica glass. When it is combined with the confinement factor, the large refractive index in silicon can provide nonlinear phase modulation such as self/cross phase modulations (SPM/XPM) at relatively low power levels and at short distances. A detailed review of SPM and XPM in silicon wire has been presented by Dadap. et al [21]. In particular, Kerr nonlinearity has been studied extensively to demonstrate SPM based broadband continuum generation, Figure 3, FWM based wavelength conversion and optical regeneration, Figure 4, [22-24]

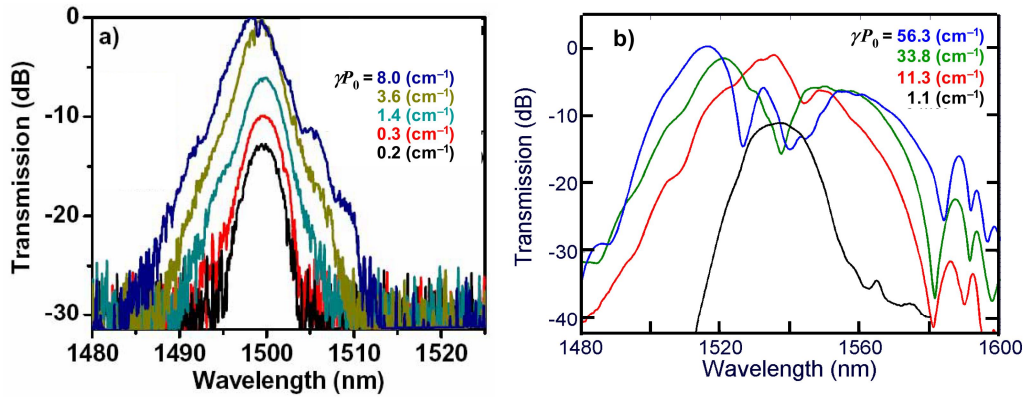


Fig. 3 The SPM induced spectrum with respect of power for (a) 1.8ps pulse [22] and (b) 200fs pulse [23].

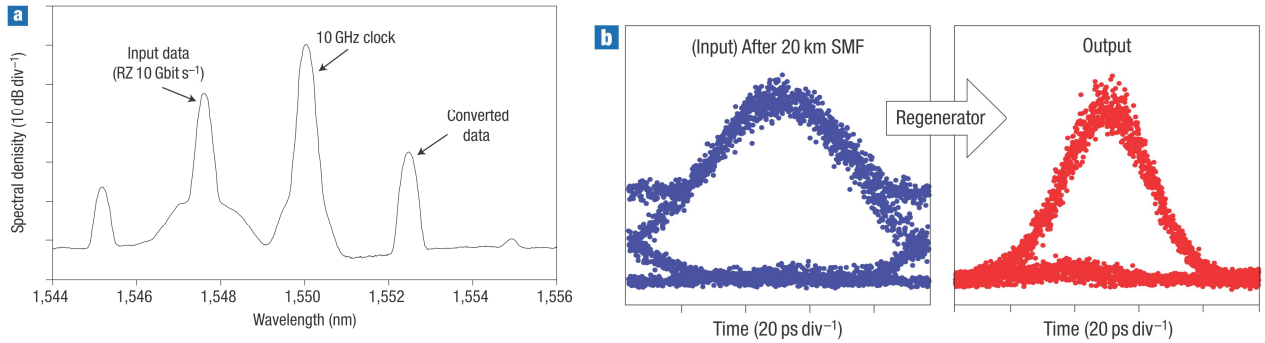


Fig. 4 (a) Spectrum of the input, clock and converted data. (b) eye diagram of the input and output signal.[24]

Cross phase modulation can also be treated as the nonlinear gating function in a frequency resolved optical gating (FROG) system. A FROG system is traditionally constructed by a second harmonic generation (SHG) autocorrelator followed by a spectrometer to extract both the amplitude and the phase information of an ultrafast optical signal. However, it is a nonlinear process and its efficiency is intensity and phase matching dependent. Since SPM and XPM have very low threshold in silicon waveguides, it can provide high sensitivity optical gating. Also, using XPM FROG mitigates the ambiguity in the direction of time of the retrieved pulse and hence XPM FROG can provide a comparable sensitivity without ambiguity [27-29].

Recently we experimentally show that XPM frog indeed can measure the phase and the amplitude of the optical pulses by using a centimeter long silicon waveguides. The schematic setup of silicon XPM FROG is shown in Fig. 5. The incident pulses are separated by a polarization beam coupler/splitter (PBC) into two polarization components that are orthogonal to each other. The ratio between two branches can be controlled by the polarization controller at the input. An optical time delay line constructed by two fiber collimators and a moving stage is used to produce time delay between two polarizations. After passing the delay line, the two polarization branches are combined by another PBC and entering

a 1.7 cm SOI waveguide. The waveguide has 5 μm2 modal area. Probe pulse is selected by a PBS at the output of the waveguide. We use an optical spectrum analyzer (OSA) to measure the spectrum and generate the spectrogram. The probe signal selected at the output of the PBS can be written as [28]:

$$E_{sig}^{SPM+XPM}(t,\tau) = E(t)\exp\left(i\gamma L\left[\frac{2}{3}\left|E(t)\right|^2 + \frac{3}{4}\left|E(t-\tau)\right|^2\right]\right) \quad (1)$$

where Ep(t), EG(t) is the field in the two polarization branches ,γ is the Kerr nonlinear coefficient, L is the length of the waveguide. If we can simplified equation (1) by assuming that the probe intensity is small and self phase modulation can be ignored. The signal intensity becomes:

$$E_{sig}^{XPM}(t,\tau) = E(t)e^{\frac{4}{3}i\gamma\left|E(t-\tau)\right|^2} \quad (2)$$

The spectrum of the signal is

$$I_{sig}^{XPM}(w,\tau) = \left|\int_{-\infty}^{\infty} E(t)e^{\frac{4}{3}i\gamma\left|E(t-\tau)\right|^2} e^{i\omega t}\right|^2 \quad (3)$$

The spectrogram is generated by measuring spectrum with different delay between two signals. The pulse amplitude and phase information then can be retrieved from the spectrogram by using principal component generalized projections (PCGP) algorithm [30]. In the PCGP algorithm some criteria of the probe and gate is required to avoid ambiguous solutions. For example, in SHG FROG the criteria is P(t)=G(t), where P(t) is the probe signal and G(t) is the gate signal of the FROG system. In the XPM FROG we treat the probe field EP as the input P(t) and the XPM exponential term exp(4/3iγ|EG(t-τ)|2) in (2) as the gate function G(t). Since the gate is only a phase modulation the amplitude of G(t) is reset to one in each itineration while keeping the phase information. In addition, the spectrogram is normalized to compensate the energy fluctuations caused by TPA and free carrier effect in silicon.

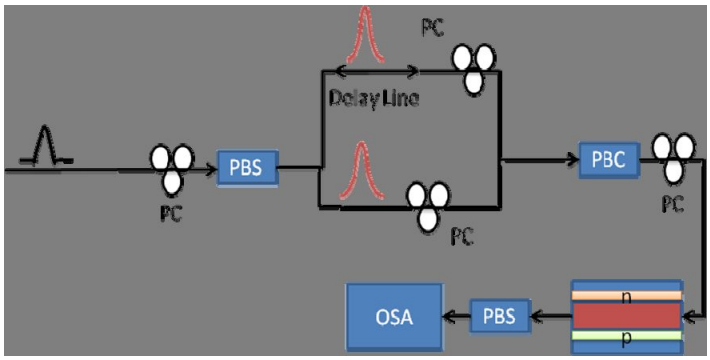


Fig. 5. Schematic setup of XPM FROG in silicon. PC: polarization controller; PBC: polarization beam coupler; OSA: optical spectrum analyzer.

The spectrogram for measuring a femtosecond modelocked fiber laser is shown in Fig. 6 (a). The spectrogram is taken within 12.8 ps time delay. The pulse is then retrieved by PCGP algorithm. The error between the measured and retrieved spectrograms is 4%. The noise is mainly due to noise in the spectrum analyzer and the interference between probe and gate pulses. The retrieved pulse and the phase are shown in Fig. 6 (a). We can see that the input pulse has a pulse width ~300 fs. The detail structure of the pedestal of the pulse is also reconstructed and resolved by the FROG system. To confirm the measurement, an autocorrelation measurement is performed by measuring the two photon absorption generated current across the p-n junction over the waveguide with respect of the time delay between two arms of the probe and gate pulses [12], Fig 7 (b).

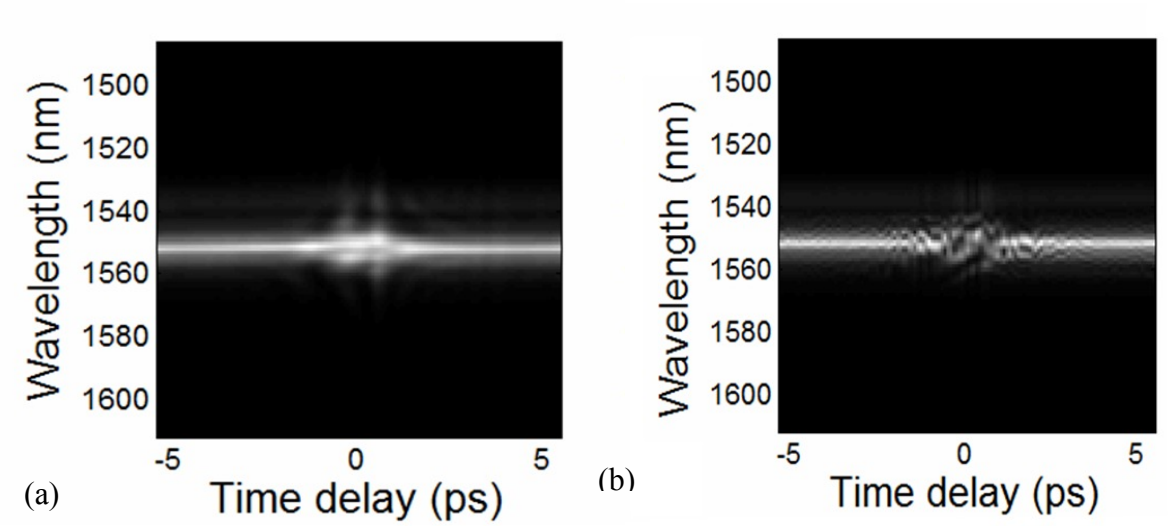


Fig. 6 (a) Retrieved spectrogram and (b) measured spectrogram

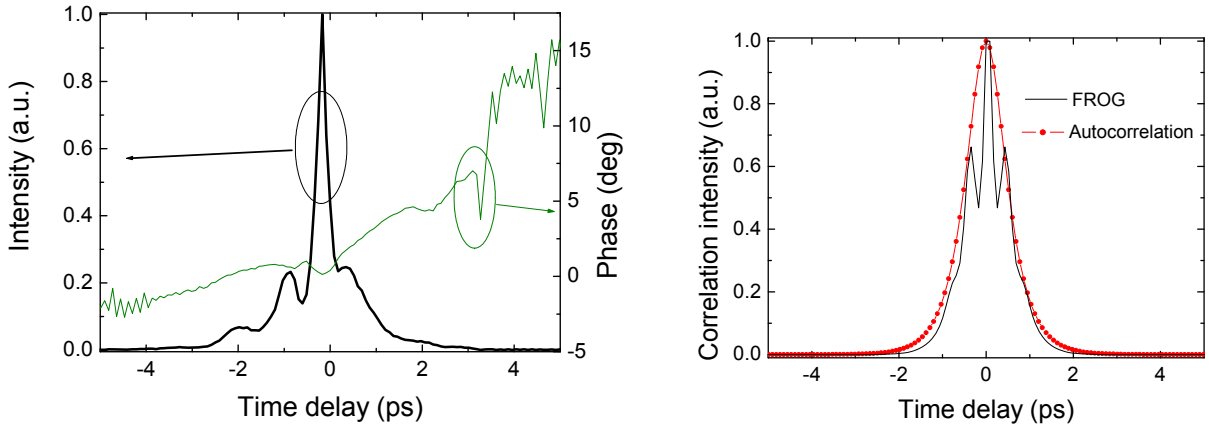


Fig. 7 (a) Retrieved pulse and phase. (b) Correlation trace of the FROG result and the autocorrelator measured result

## 4. TWO PHOTON ABSORPTION BASED SILICON DEVICES

### 3.1 Two-photon absorption and TPA-induced free carrier absorption

Two-photon absorption (TPA) and TPA-induced free carrier absorption (FCA) are two ubiquitous nonlinear effects in silicon for any wavelength between 1.1 μm and 2.2 μm. TPA in silicon is a memoryless nonlinear process related to the intensity square as estimated by the nonlinear Schrödinger equation [10, 14]:

$$\frac{\partial E(t,z)}{\partial z} = -\frac{1}{2}\left\{ \alpha + \alpha_{FCA}(t,z) + \alpha_{TPA}(t,z) \right\} E(t,z) - i\gamma \left|E(t,z)\right|^2 E(t,z) + i\frac{2\pi}{\lambda}\Delta n(t,z)\, E(t,z) \tag{4}$$

Here the parameters *E(t,z)* represent the electric-field, $\alpha$ is the attenuation constants, $\gamma$ is the effective nonlinearity and $\Delta n$ is the free carrier induced index change, respectively. Among two nonlinear loss terms, the TPA,

$$\alpha_{TPA} = \frac{1}{z}\ln(1+\beta I_0 z) \tag{5}$$

follows the pulse shape. Here $\beta$ is the TPA coefficient (0.7 cm/GW at 1550nm [18]), $A_{eff}$ is the effective area of the waveguide and Io is the intensity. The free carriers are on the other hand accumulative and induce index change and absorption, as follows:

$$\alpha_{FCA} = -\left[8.5\times10^{-18}\Delta N_e + 6\times10^{-18}\Delta N_h\right] \quad (6)$$

$$\Delta n = -\left[8.8\times10^{-22}\Delta N_e + 8.5\times10^{-18}\Delta N_h^{\,0.8}\right] \quad (7)$$

Where $\Delta N_e$ and $\Delta N_h$ are electron and hole concentration change, respectively. Since TPA always generate electron and hole pairs, $\Delta N_e$ and $\Delta N_h$ can be replace by only $\Delta N$. Near wavelength around 1.55 μm, the absorption coefficient can be derive [13]:

$$\alpha_{FCA}(z,t) = 1.45\times10^{-17}\left(\frac{\lambda}{1.55}\right)^2 N(z,t)\ \left(\mathrm{cm}^{-1}\right) \quad (6)$$

For CW signals or time varying signals wider than free carrier recombination time, $\tau_o$, free carrier densities will be stabilized at a local *N(z)* value of: $N(z)=\tau_o\cdot\beta\cdot I^2(z)/2h\upsilon$ after $\sim\tau_o$. On the other hand, time varying optical signals with pulse width smaller than $\tau_o$ will result in different time dependent local free carrier densities and TPA induced FCA along the waveguide governed by the equation:

$$\frac{dN(t,z)}{dt} = -\frac{N(t,z)}{\tau_0} + \beta\frac{I^2(t,z)}{2h\upsilon} \quad (7)$$

Although, the free carrier absorption is detrimental to many applications, the time varying property of free carrier density, as indicated in the equation (1), can be an asset for ultrafast pulse shaping. For instance, we can control the attenuation at the trailing edge of a pulse by using the free carriers generated by the leading edge. Fig. 8 illustrates the schematic diagram of pulse propagation in a silicon waveguide and the proposed concept where free-carrier losses are significant, and also the amount of free-carrier-induced losses. Upon entering the waveguide the front end of the pulse will be slightly attenuated by TPA and hence the free carriers will start to accumulate wherever the optical energy is present. As a result, the photons entering the waveguide will suffer from the free-carrier losses generated by the earlier photons. This process will lead to attenuation of the trailing edge of the pulse and hence the pulse compression in the time domain, (see Fig. 8(a)). Because of the linear and nonlinear absorption, the free-carrier absorption will be spatially

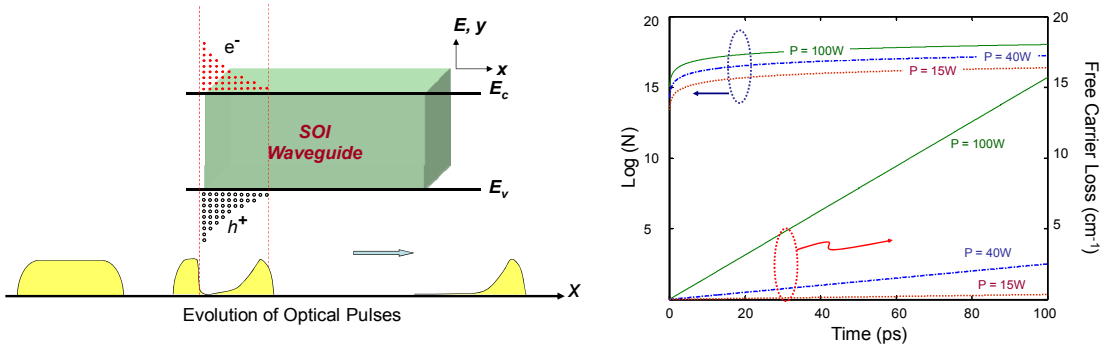


Fig. 8. (a) Schematic description of free-carrier accumulation for pulse compression. A high-intensity optical pulse will leave paint of free carriers behind, which will contribute to pulse attenuation at the trailing edge and hence compression. (b) Temporal variation of free-carrier concentration and losses generated by 100ps optical pulses. The loss difference between the front and end of the pulse can be as high as 16cm$^{-1}$ for optical pulses with 100W peak power values.

varying and will be much stronger at the input facet of the silicon waveguide. Fig. 8(b) quantifies the loss and free-carrier accumulation along a 100ps rectangular pulse to give a better understanding of the concept. The results presented here are calculated for a silicon waveguide with 5 $\mu m^2$ effective area, similar to the one used in the experiment, for three different peak power values of 100W, 40W and 15W. At the front facet of the waveguide, an optical pulse with 100 W peak power level is expected to create free carriers, the free carrier density increased from 0 to $>10^{19}$ $cm^{-3}$ from beginning time (t=0) to end of the pulse (t=100 ps). As a result, the trailing edge of the pulse is expected to experience 16 $cm^{-1}$ free-carrier-induced loss at that position while the leading edge travels with only TPA loss. The same loss value reduces to ~3 $cm^{-1}$ if the input peak power is reduced to 15W.

The free carrier induced dispersion has also been exploited to illustrate micron size optical switches. Fig. 9 shows an example of such a switch activated by fast modulation in carrier injection rate [31-32]. In this example, a strong optical control pulse and a weak CW signal light are coupled into the resonator though two different resonance. Free carrier is generated by TPA when the control pulse is present and the refractive index is reduced and blue shift the resonance frequency. As a result the CW signal is then modulated by the control pulse. By applying two input control signal with carefully adjust the wavelength, an AND/NAND gate is demonstrated [32]. Other than free carrier effect, TPA itself can be used as a cross absorption modulation scheme [33]. A autocorrelation measurement has been realized for pulse characterization [34].

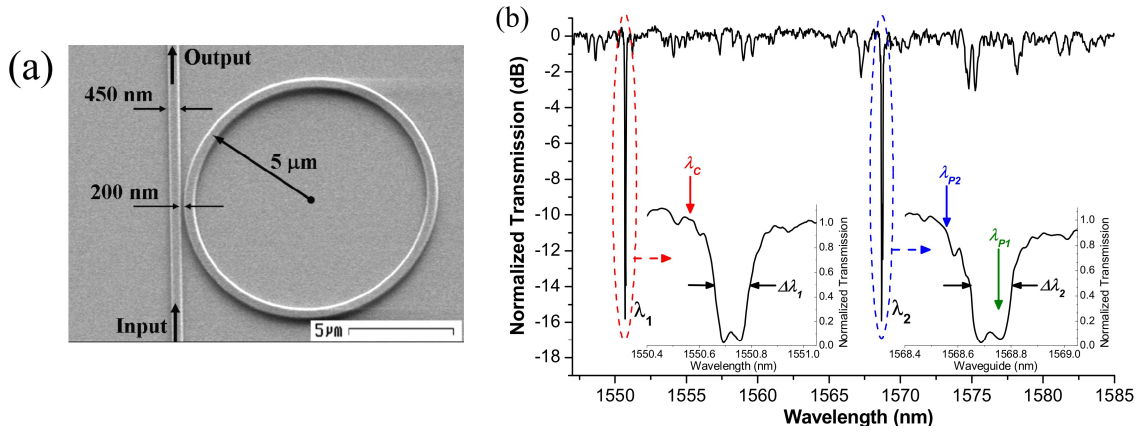


Fig. 9 (a) A silicon ring resonator and (b) the operation wavelengths for the logic gate.

The free-carrier absorption can also be utilized to demonstrate laser modelocking and short pulse generation by using silicon waveguides. First, an optical modulation is needed to initiate pulsation in the cavity to increase peak power and start free-carrier transients. This modulation can be performed by using the silicon waveguide itself [4, 10-11] or bulk electro-optic modulators. In the second step, this pulse is amplified by a gain medium and then compressed by free carriers. The pulse compression will occur at the leading edge of the pulse by suppressing the trailing edge due to free-carrier absorption. In the third step, recirculation of this pulse helps to form short pulses at the steady state. Conventionally, passively modelocked lasers require saturable absorbers to suppress the low intensity background and initiate oscillation of intensity spikes. The active modelocked lasers, on the other hand, require optical modulators to initiate pulsation at harmonics of the fundamental cavity frequency. In order to create short pulses, the modulation signal has to be short. The free-carrier absorption can alleviate the short pulse modulation requirement if it is used as a pulse shaping mechanism inside the laser cavity. The modulation part of our scheme resembles the active modelocking. However, free-carrier absorption behaves like a saturable absorber on the trailing edge and provides unique pulse shaping method inside the cavity.

For pulse shaping, time and space dependent free carrier density, $N(z,t)$, and the nonlinear losses are the utmost important parameters to be determined. Based on the peak intensity and the pulse energy, the nonlinear response of silicon can be divided into two separate regimes in time and in space: TPA dominated regime and FCA dominated regime [14]. Fig. 10 illustrates the calculated outcome of two different regimes for 20ps and 500ps optical pulses with 1 kW peak power (i.e. 20 nJ and 500 nJ pulse energies). The waveguide is set to be 1 cm long with 5 $\mu m^2$ effective area and 16ns free carrier lifetime. The fixed 1 kW peak power facilitates the same level of TPA (90%) at the center for comparison, Fig. 10(a). However, FCA generated by 500 nJ pulse is 40x stronger than the FCA generated by 20 ps pulses at the same peak intensity due to difference in number of absorbed photons. We estimate that while 20 nJ pulses are being broadened due to the TPA dominance, 500nJ pulses are being compressed to 350 ps by FCA dominance, Fig 10(b). Here results are presented in normalized time unit, $t/\tau_{FWHM}$, where $\tau_{FWHM}$ is the pulse width at the waveguide input, to have better comparisons of output pulses for different input conditions and to have better visualization. The free carrier plasma effect is always present and, unlike FCA and TPA competition, produces a steady linear phase change across the pulse. However, due to the larger free carrier density, high energy pulses experience ~4x larger phase change across the pulse, Fig. 10(b). A blue shifted spectral broadening has been attributed to this phase change when it is combined with self phase modulation, as previously shown [10].

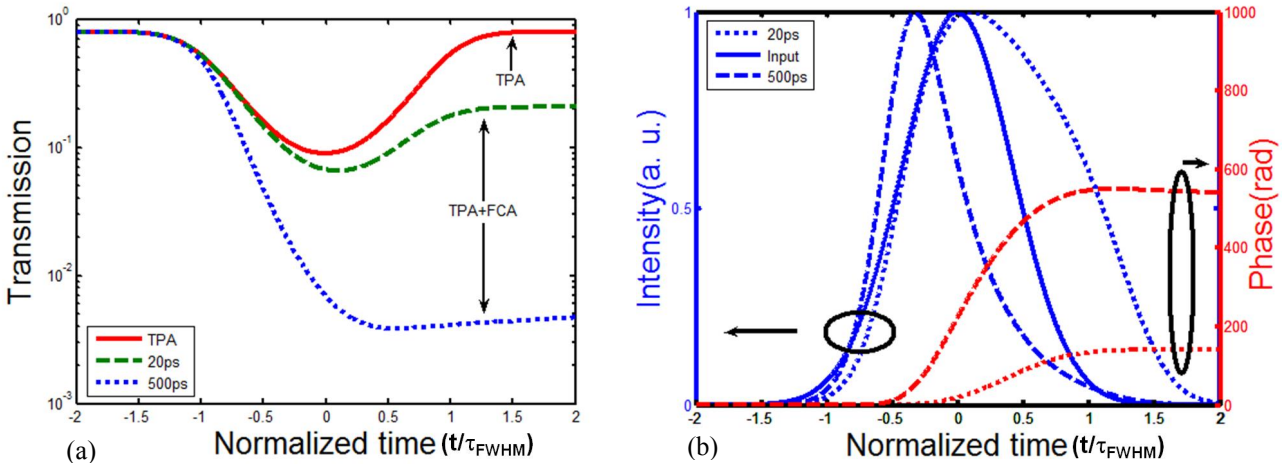


Fig. 10. (a) TPA and free carrier loss profiles of 20 ps and 500 ps wide input pulses. (b) Estimated output pulses and chirp induced by free carrier plasma effect. The font end of both pulses are under TPA dominant nonlinear regime. However, due to excess free carriers, the trailing edge of 500 ps pulse is under FCA dominant nonlinear regime.

The losses presented here represent aggregate attenuation at the end of the waveguide. We expect that the total length of the waveguide, input pulse width and the pulse energy will have prominent influence on the final outcome. Fig. 11(a) illustrates the compression behavior of 10ps to 1000ps optical pulses in a 1cm long silicon waveguide. At low peak powers, $< 10^{16}$ $cm^{-3}$ carriers are generated to facilitate attenuation of the trailing edge and to provide self compression [13]. However, stronger TPA at the center of the pulse dominates at these intensities and induces net pulse broadening at 3dB point. Free carrier dominance is expected at higher intensities. For example, 1ns pulses with 2 $GW/cm^2$ intensities generate $4\times10^{18}$ $cm^{-3}$ free carriers which dominate over TPA at the center of the pulse and facilitate net self compression. For 500ps and 100ps wide optical pulses, it requires 3 $GW/cm^2$ (75nJ) and 32 $GW/cm^2$ (160nJ) to initiate the same type of compression, respectively. For input pulses shorter than 50ps, TPA induced pulse broadening surpasses the self compression even at 40 GW/cm2 and hence net pulse broadening is expected. However, we should note that, simple free carrier density calculations may not be reliable at such a high intensities due to Auger recombination [27]. For instance, as the free carrier density increases from $10^{18}$ $cm^{-3}$ to $10^{19}$ $cm^{-3}$ the free carrier lifetime due to Auger effect will reduce

from ~1.3 μs to ~20 ns, which is comparable to free carrier lifetime of our waveguides. Fig. 11(b) demonstrates the effect of waveguide length on the pulse compression. For longer waveguides, the front end of the waveguide facilitate FCA dominated nonlinear behavior with $>10^{18}$ $cm^{-3}$ free carriers. The back end, on the other hand, operates in TPA dominated regime and contributes mostly on pulse broadening and loss. Specifically, the free carrier density at the trailing edge of a 100ps pulse is estimated to be $\sim10^{19}$ $cm^{-3}$ at the input facet. The same density drops to $10^{18}$ $cm^{-3}$ and to $2x10^{17}$ $cm^{-3}$ at L=2 mm and at L=10 mm, respectively. As a result, the largest compression occurs within the first ~2 mm due to FCA dominance, and then TPA induced pulse broadening dominate in the following ~8 mm waveguide segment. Hence, for 100 ps input pulses, the waveguides as short as 2 mm can provide more effective pulse compression with only 50% of peak power values used in 1cm. These results indicate that effective utilization of TPA and FCA requires optimization of the waveguide geometry for desired pulse parameters.

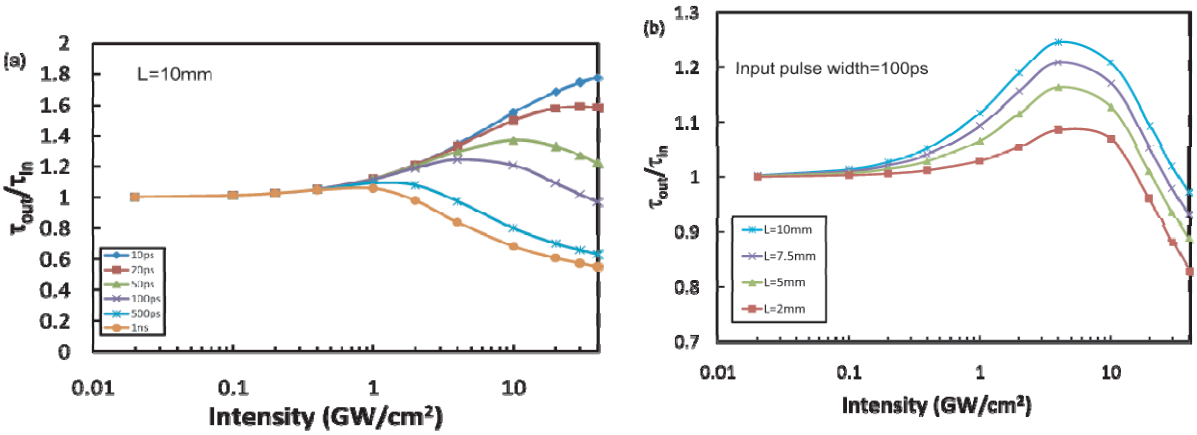


Fig. 11. Predicted pulse compression ratio in (a) 10 mm long silicon waveguide for different initial pulse widths and (b) silicon waveguides with different lengths.

### 3.2 Laser modelocking and pulse compression experiment results

Modelocking experiment of the pulse compression in silicon is demonstrated in a laser cavity formed by an erbium doped fiber amplifier (EDFA) gain medium, a silicon pulse compressor and a spool of standard fiber as illustrated in Fig. 12. The silicon waveguide used for pulse compression is a 1.7cm long silicon on insulator waveguide with ~5μm$^2$ effective area. The total fiber-to-fiber loss of the waveguide is measured to be ~2dB. The output of the waveguide is connected to a 10/90 tap coupler where 10% used as an output and 90% is fed into the gain medium, a high power EDFA with 200 mW saturated output power. The resonator is formed by launching the EDFA output back into the silicon waveguide input. Since the pulse shaping by free carriers requires a time-dependent optical signal circulating inside the cavity, an 8 ns pulsed current source is connected to the waveguide to start initial pulsation at the fundamental cavity frequency of ~1.4MHz. The output pulse width is expected to be minimized when the frequency of the function generator matches the fundamental cavity frequency. Here, manual frequency locking is achieved by monitoring the pulse shape and the modulation frequency, simultaneously. The output of the resonator is connected to an optical spectrum analyzer and a photodetector followed by a 25GHz sampling oscilloscope or an RF spectrum analyzer to measure output characteristics. Since the pulse compression is intensity square dependent, at constant pulse width, the variation of rise and fall time can be used to tune the pulse energy and hence the number of free carriers generated by an optical pulse at fixed peak power.

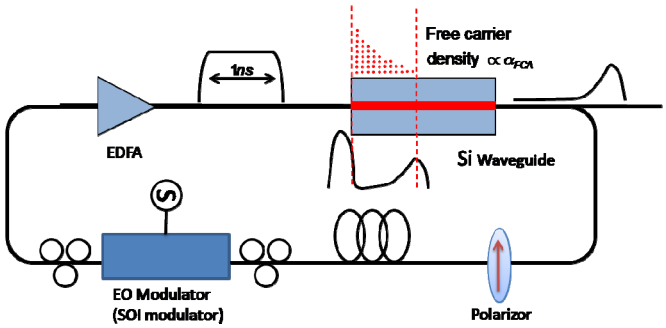


Fig. 12. Experimental setup used for TPA based modelocking and pulse compression scheme. SOI: Silicon on insulator waveguide, EDFA: erbium doped fiber amplifier

Fig. 13(a) illustrates the pulse widths measured at the laser output for different peak powers and different rise/fall times. The shortest pulse width is measured to be 60 ps by using RF signals with 140ps rise/fall time. Fig. 13(b) shows the tendency of the pulse compression with respect to different peak powers and different rise/fall times. At fixed pulse energy, slower rise time results in fewer free carrier generation. As a result, the pulse width increases to 85ps if the rise time is tuned to 650ps for the same pulse energy. These measurements indicate that free carrier concentration increases more rapidly for modulation signals with sharper rise times. To compensate the slope effect we need to increase pulse energy to achieve the same compression, as shown in Fig. 13(b). This tendency agrees with the theoretical results presented in Fig. 13(a), which shows the higher peak power requirement for low energy pulses. For instance, to achieve 80 ps output pulses, the average power entering the silicon waveguide has to be maintained at 9dBm, 13dBm and 16dBm levels for 140 ps, 450 ps and 650 ps rise and fall times, respectively. The peak power corresponding to 80ps pulse with 9 dBm average power is ~120 W (2.4G W/cm$^2$). The total loss at this setting is measured to be <6dB, of which 2dB is the linear loss and the rest originates from the nonlinear effects.

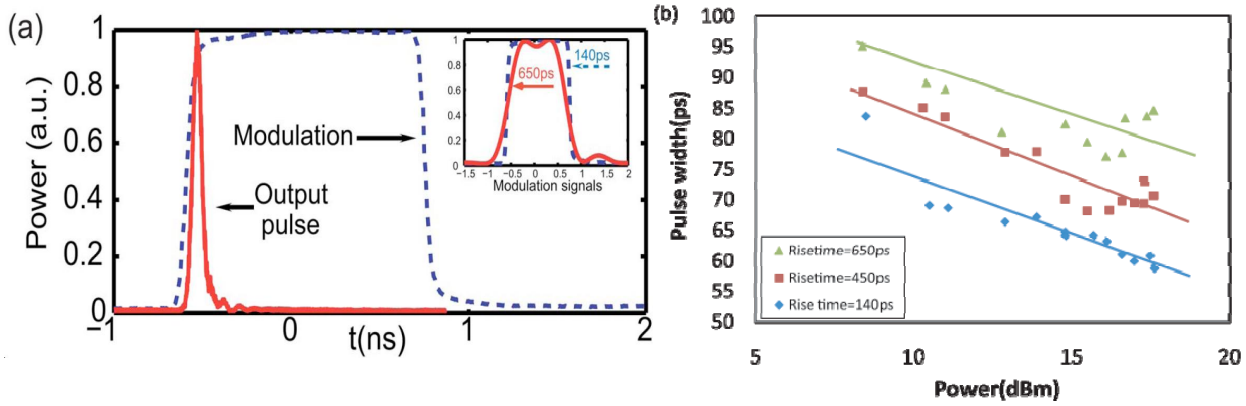


Fig. 13. (a) Laser output and the 1.5 ns modulation with 140 ps rise time. (Inset) Modulation signals used for modelocking experiment. (b) Variation of output pulse width with respect to pulse energy.

### 3.3 Raman amplification and dual wavelength short pulses lasing using compressed pulses

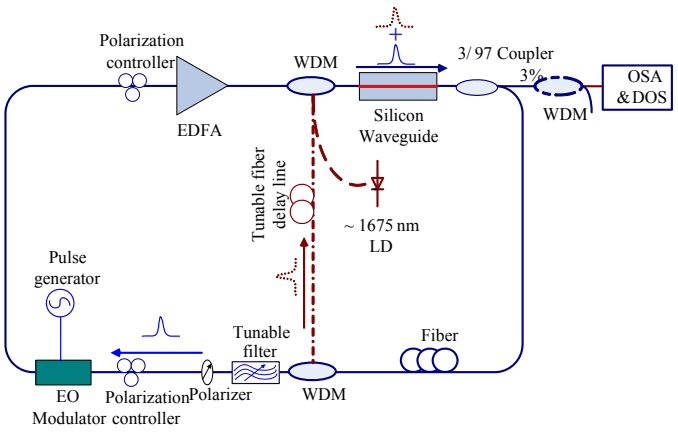


Fig. 14. Experimental setup for testing Raman amplification and dual wavelength lasing

Net gain amplification and lasing in silicon have been previously demonstrated using a pulsed-pumping technique [1,3]. To study stimulated Raman scattering inside the modelocked laser cavity, a simple pump-probe experiment is conducted by using a continuous wave (CW) probe laser around 1675 nm. The setup is shown in Fig. 14. In this experiment, Raman gain inside the laser cavity is measured for various pulsing conditions. We show that a 2.8 dB Raman gain can be measured at the front end of a long pulse with a large pedestal when the modelocking condition is not optimized, as shown in Fig. 15. However, at the same time, the pulse suffers from a 7 dB free carrier loss at the trailing edge. Hence, for low loss and an effective Raman effect, the fundamental pulse modelocking should be optimized before the Raman cavity is formed.

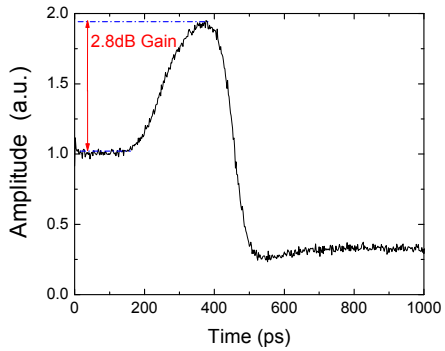


Fig.15. Raman gain pumped with compressed pulses

The observation of a 2.8 dB gain indicates that a careful design of the laser cavity can facilitate lasing at the Stokes wavelength by stimulated Raman scattering without an additional pump and hence enhance the functionality of the silicon chip [28]. Because of wavelength selectivity of the filter, another cavity for Raman Stokes pulse is needed. To facilitate resonance at the pump wavelength and the Stokes wavelength, the experimental setup is modified according to dashed line in Fig. 14. After removing the probe CW laser, the original laser cavity is modified by using two WDM couplers, which separate the Stokes from the wavelength sensitive components in the pulse compression cavity and recombine before the silicon waveguide, and a tunable fiber delay. Once modelocking is optimized to generate short pulses, we are able to utilize the short pulses as the pump to achieve stimulated Raman scattering and modelocking in the second cavity. After pulses at both wavelengths are aligned temporally, we observe lasing at Stokes and pump

wavelengths. The spectra of the dual wavelength laser are shown in Fig. 16. The pump wavelength is selected by the band pass filter inside the laser cavity to be 1540 nm and the expected Raman Stokes signal is at wavelength of 1675 nm [3].

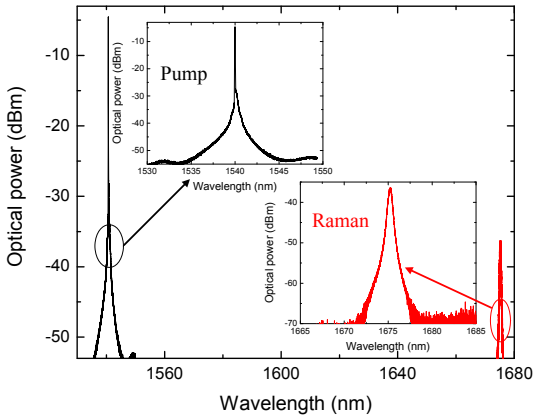


Fig.16. Spectra of the pulse-compressed pump and Raman laser

## 4. CONCLUSION

A review for recent development of nonlinear optical effect in silicon on pulse shaping and characterization has been presented. Nonlinear effect including Raman scattering, SPM, XPM, FWM, TPA and free carrier is explained for various applications.

## REFERENCES


[1] L. Ansheng, R. Haisheng, R. Jones *et al.*, "Optical amplification and lasing by stimulated Raman scattering in silicon waveguides," Journal of Lightwave Technology 24(3), 1440 (2006).

[2] O. Boyraz, and B. Jalali, "Demonstration of 11dB fiber-to-fiber gain in a silicon Raman amplifier," IEICE Electronics Express 1(14), 429 (2004).

[3] O. Boyraz, and B. Jalali, "Demonstration of a silicon Raman laser," Optics Express 12(21), 5269 (2004).

[4] H. Rong, A. Liu, R. Jones *et al.*, "An all-silicon Raman laser," Nature 433(7023), 292-294 (2005).

[5] A. Liu, R. Jones, L. Liao *et al.*, "A high-speed silicon optical modulator based on a metal-oxide-semiconductor capacitor," Nature 427(6975), 615-618 (2004).

[6] A. Liu, L. Liao, D. Rubin *et al.*, "High-speed optical modulation based on carrier depletion in a silicon waveguide," Optics Express 15(2), 660-668 (2007).

[7] V. Raghunathan, R. Claps, D. Dimitropoulos *et al.*, "Parametric Raman wavelength conversion in scaled silicon waveguides," Journal of Lightwave Technology 23(6), 2094-2102 (2005).

[8] K. Yamada, H. Fukuda, T. Tsuchizawa *et al.*, "All-optical efficient wavelength conversion using silicon photonic wire waveguide," IEEE Photonics Technology Letters 18(9), 1046-1048 (2006).

[9] K. K. Tsia, S. Fathpour, and B. Jalali, "Energy harvesting in silicon wavelength converters," Optics Express 14(25), 12327-12333 (2006).

[10] Boyraz, P. Koonath, V. Raghunathan *et al.*, "All optical switching and continuum generation in silicon waveguides," Optics Express 12(17), 4094-4102 (2004).

[11] V. R. Almeida, C. A. Barrios, R. R. Panepucci *et al.*, "All-optical control of light on a silicon chip," Nature 431(7012), 1081-1084 (2004).

[12] V. R. Almeida, C. A. Barrios, R. R. Panepucci *et al.*, "All-optical switching on a silicon chip," Optics Letters 29(24), 2867-2869 (2004).

[13] E. K. Tien, N. S. Yuksek, F. Qian *et al.*, "Pulse compression and modelocking by using TPA in silicon waveguides," Optics Express 15(10), 6500-6506 (2007).
[14] E. K. Tien, F. Qian, N. S. Yuksek *et al.*, "Influence of nonlinear loss competition on pulse compression and nonlinear optics in silicon," Applied Physics Letters 91, 201115 (2007).
[15] Y. Okawachi, M. Foster, J. Sharping *et al.*, "All-optical slow-light on a photonic chip," Optics Express 14(6), 2317-2322 (2006).
[16] F. Xia, L. Sekaric, and Y. Vlasov, "Ultracompact optical buffers on a silicon chip," Nature Photonics 1(1), 65 (2007).
[17] T. Liang, L. Nunes, T. Sakamoto *et al.*, "Ultrafast all-optical switching by cross-absorption modulation in silicon wire waveguides," Optics Express 13(19), 7298-7303 (2005).
[18] V. Raghunathan, D. Borlaug, R. R. Rice et al., "Demonstration of a mid-infrared silicon Raman amplifier," Optics Express, 15(22), 14355-14362 (2007).
[19] B. Jalali, V. Raghtmathan, R. Shori et al., "Prospects for silicon mid-IR Raman lasers," Ieee Journal Of Selected Topics In Quantum Electronics, 12(6), 1618-1627 (2006).
[20] H. S. Rong, S. B. Xu, O. Cohen et al., "A cascaded silicon Raman laser," Nature Photonics, 2(3), 170-174 (2008).
[21] J. I. Dadap, N. C. Panoiu, X. Chen *et al.*, "Nonlinear-optical phase modification in dispersion-engineered Si photonic wires," Opt. Express, 16(2), 1280 (2008).
[22] I. W. Hsieh, X. Chen, J. I. Dadap *et al.*, "Ultrafast-pulse self-phase modulation and third-order dispersion in Si photonic wire-waveguides," Opt. Express, 14(25), 12380 (2006).
[23] E. Dulkeith, Y. A. Vlasov, X. Chen *et al.*, "Self-phase-modulation in submicron silicon-on-insulator photonic wires," Opt. Express, 14(12), 5524 (2006).
[24] R. Salem, M. A. Foster, A. C. Turner *et al.*, "Signal regeneration using low-power four-wave mixing on silicon chip," Nat Photon, 2(1), 35 (2008).
[25] W. Mathlouthi, H. Rong, and M. Paniccia, "Characterization of efficient wavelength conversion by four-wave mixing in sub-micron silicon waveguides," Opt. Express, 16(21), 16735 (2008).
[26] A. C. Turner, M. A. Foster, A. L. Gaeta *et al.*, "Ultra-low power parametric frequency conversion in a silicon microring resonator," Opt. Express, 16(7), 4881 (2008).
[27] M. D. Thomson, J. M. Dudley, L. P. Barry, and J. D. Harvey, "Complete pulse characterization at 1.5 □m by cross-phase modulation in optical fibers," *Opt. Lett.*, vol. 23, pp. 1582, 1998.
[28] P. Honzatko, J. Kanka, and B. Vrany, "Measurement of pulse amplitude and phase using cross-phase modulation in microstructure fiber," *Optics Letters*, vol. 30, pp. 1821-1823, 2005.
[29] D. Reid, P. J. Maguire, L. P. Barry, Q.-T. Le, S. Lobo, M. Gay, L. Bramerie, M. Joindot, J.-C. Simon, D. Massoubre, J.-L. Oudar, and G. Aubin, "All-optical sampling and spectrographic pulse measurement using cross-absorption modulation in multiple-quantum-well devices," *J. Opt. Soc. Am. B*, vol. 25, pp. A133, 2008.
[30] D. J. Kane, "Real-time measurement of ultrashort laser pulses using principal component generalized projections," *Selected Topics in Quantum Electronics, IEEE Journal of*, vol. 4, pp. 278, 1998.
[31] Q. Xu, and M. Lipson, "All-optical logic based on silicon micro-ring resonators," Opt. Express, 15(3), 924 (2007).
[32] S. Preble, Q. Xu, B. Schmidt *et al.*, "Ultrafast all-optical modulation on a silicon chip," Opt. Lett., 30(21), 2891 (2005).
[33] T. K. Liang, L. R. Nunes, M. Tsuchiya *et al.*, "High speed logic gate using two-photon absorption in silicon waveguides," Optics Communications, 265(1), 171-174 (2006).
[34] T. K. Liang, H. K. Tsang, I. E. Day *et al.*, "Silicon waveguide two-photon absorption detector at 1.5 μm wavelength for autocorrelation measurements," Applied Physics Letters 81, 1323 (2002).